Engineering Failure Analysis 16 (2009) 273–280

Contents lists available at ScienceDirect

Engineering Failure Analysis

journal homepage: www.elsevier.com/locate/engfailanal

Degradation of turbine blades and vanes by overheating in a power station

H.M. Tawancy *, Luai M. Al-Hadhrami

Center for Engineering Research, Research Institute, King Fahd University of Petroleum and Minerals, P.O. Box 1639, Dhahran 31261, Saudi Arabia

ARTICLE INFO

Article history:
Received 26 February 2008
Accepted 26 May 2008
Available online 7 June 2008

Keywords:
Turbine blades
Vanes
Failure
Microstructure
Overheating

ABSTRACT

First-stage turbine blades and vanes were fractured after 18,420 h of operation at about 800 °C in a power station. Overheating was found to be the cause of failure as indicated by microstructural characterization using various electron-optical techniques. This was indicated by coarsening and rafting of the strengthening γ′-phase in the nickel-base blade material as well as the presence of a continuous network of grain boundary carbides. For the cobalt-base vane material, overheating was indicated by decomposition of MC-type carbides and formation of a cellular structure of Laves phase at grain boundaries. Fracture of both the blades and vanes was found to occur by a mixed mode involving intergranular cracking and fatigue. Most evidence pointed out that initial damage by creep resulting in intergranular cracking had shortened the fatigue life of blades and vanes.

1. Introduction

Materials used in gas turbine blade and vane applications are subject to degradation during service by the combined effects of temperature, mechanical stresses, and environmental conditions [1–3]. Various degradation modes include cracking, creep damage, fatigue, loss of thermal stability (precipitation of undesirable phases during extended exposure at elevated temperatures), and environmental attack (oxidation and hot corrosion). Some of these modes, however, are interrelated, and can occur simultaneously. For example, cracking can occur by creep and/or fatigue mechanisms. It is well known that creep damage can significantly reduce the fatigue strength [4]. Furthermore, cracking by these mechanisms can be promoted by environmental attack and/or loss of thermal stability.

In practice, damage of hot section components such as blades and vanes is accelerated by overheating due to: (i) higher than normal operating temperature, (ii) damage of exit holes of cooling air by creep deformation in the case of air-cooled blades, and (iii) blockage of air cooling channels by various contaminants such as sand particles due to improper filtering of incoming air. Also, uneven distribution of temperature, which may contribute to thermal–mechanical fatigue can result from misfiring due malfunction of the burner [5].

It was the objective of this study to analyze the degradation modes of first stage turbine blades and vanes used in a power station employing various electron-optical techniques. The internally-cooled blades were made of the nickel-base Udimet[1] alloy 710 (Ni–18Cr–15Co–5Ti–3Mo–2.5Al–0.07C in wt%), and the cobalt-base alloy MAR M[2] 918 (Co–20Ni–20Cr–7.5Ta–0.05C) was used in the vane application. After 18,420 h of operation (less than one-half of the expected service life) at a temperature of about 800 °C, the engine suddenly tripped due to high vibration. Subsequent inspection revealed that a number of first stage blades were fractured and airfoils of corresponding vanes were missing.

* Corresponding author. Tel.: +966 3 860 4317.
E-mail address: tawancy@kfupm.edu.sa (H.M. Tawancy).

[1] Udimet is a trademark of the Inco family of companies.

[2] MAR M is a registered trademark of Martin Marrieta.

1350-6307/$ - see front matter © 2008 Elsevier Ltd. All rights reserved.
doi:10.1016/j.engfailanal.2008.05.001

2. Experimental procedure

Representative metallographic samples were prepared from as received blade and vane for microstructural characterization of the exposed fracture surfaces and along the cross-sections. Although oxidation of the fracture surface precluded detailed fractography, some important morphological features could be revealed after descaling. Scanning electron microscopy (SEM) combined with energy dispersive X-ray spectroscopy (windowless detector capable of detecting light elements down to carbon) and analytical electron microscopy (AEM) were used to examine the microstructures. All AEM work was carried out at an accelerating voltage of 200 kV. Thin foils for the transmission electron microscopy (TEM) and scanning transmission electron microscopy (STEM) modes were prepared by the jet polishing technique.

3. Results and discussion

3.1. Macroscopic features of damaged blade and vane

Photographs illustrating characteristic macroscopic features of the damaged blade in the as-received condition are shown in Fig. 1. It is observed that the airfoil was severely distorted and that fracture occurred along two sections normal to the direction of maximum tensile stress. Evidently, fracture was preceded by macroscopic plastic deformation, which could occur by creep suggesting that the blade was exposed to higher than normal temperatures. Distortion of the cooling air channels is noted in Fig. 1b and also in Fig. 2. Another indication that the blade was exposed to higher temperatures was extensive oxidation of the fracture surface as shown in the macrograph of Fig. 2. Usually, oxidation of Ni-based superalloys becomes significant at temperatures $\geqslant$1000 °C [6].

An example illustrating the general appearance of damaged vane is shown in Fig. 3. Similar to the case of blade described above, the surface exposed by fracture of the airfoil was heavily oxidized indicating that the vane was exposed to higher than normal temperatures.

To summarize, visual inspection of the damaged blade and vane suggested that overheating appeared to be responsible for the failure. This could be due to excessive operating temperatures and/or blockage of the cooling air channels. As shown later, microstructural characterization provided an evidence that the damage was caused by overheating.

3.2. Characteristic microstructural features of the blade and vane materials

Fig. 4 summarizes characteristic microstructural features of the blade material as observed on the scale of scanning electron microscopy. As expected, the matrix phase contained a dispersion of the strengthening γ'-phase. However, a rather continuous layer of secondary precipitates are observed to delineate the grain boundaries as shown in the backscattered

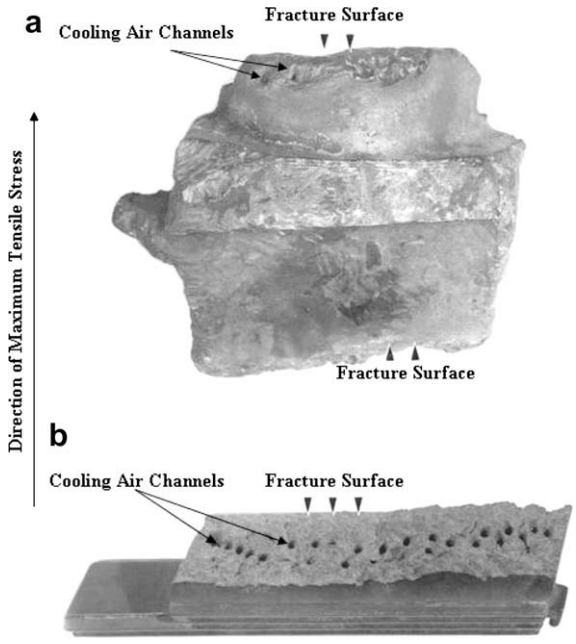

Fig. 1. Photographs illustrating the fractured blade in the as-received condition. (a) A view of the airfoil showing macroscopic distortion. (b) A view of the lower section of the fracture surface showing the cooling air channels.

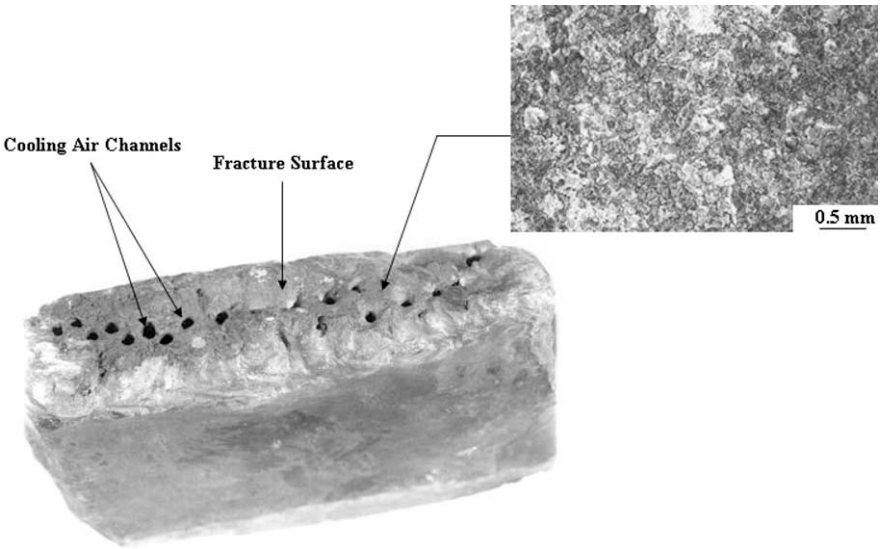

Fig. 2. A photograph showing the lower fracture surface of the blade, and corresponding secondary electron macrograph illustrating the surface oxide layer.

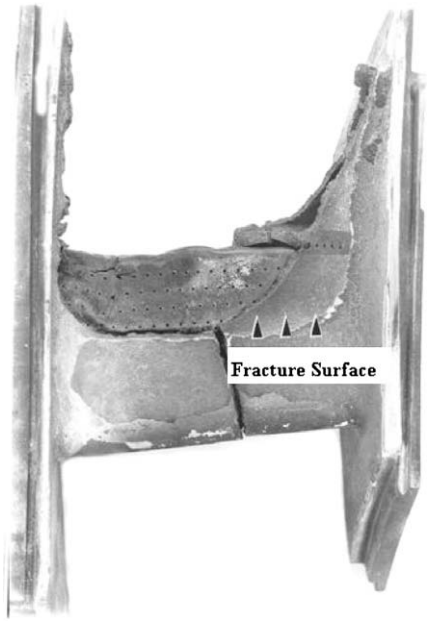

Fig. 3. A photograph showing a general view of the vane and the surface exposed by fracture of the airfoil.

electron image of Fig. 4a. A typical energy dispersive X-ray spectrum illustrating the elemental composition of the matrix phase is shown in Fig. 4b. Quantification of the spectral data showed that the composition was consistent with that of Udimet alloy 710 as specified. As shown in the spectrum of Fig. 4c, the grain boundary phase appeared to be an MC-type carbide of the form (Ti, Mo)C similar to the case of Udimet alloy 500 [7]. A carbide morphology such as that shown in Fig. 4a could have an adverse effect on mechanical strength resulting in embrittlement of the alloy [1]. Secondary intergranular cracks were observed along grain boundaries containing carbide precipitates as shown later.

Although carbides provide a source for strengthening, the exact effect is dependent upon their morphology [8]. Strengthening is most effective when the carbides are present as a dispersion within the matrix phase and as discrete particles at grain boundaries. Rapid coarsening of the carbides, however, occurs at higher temperature resulting in considerable grain boundary embrittlement. Therefore, the carbide morphology shown in the example of Fig. 4a is another indication that the blade was exposed to higher than normal temperatures. A further evidence for overheating is provided by the morphology of the strengthening γ'-phase as demonstrated below.

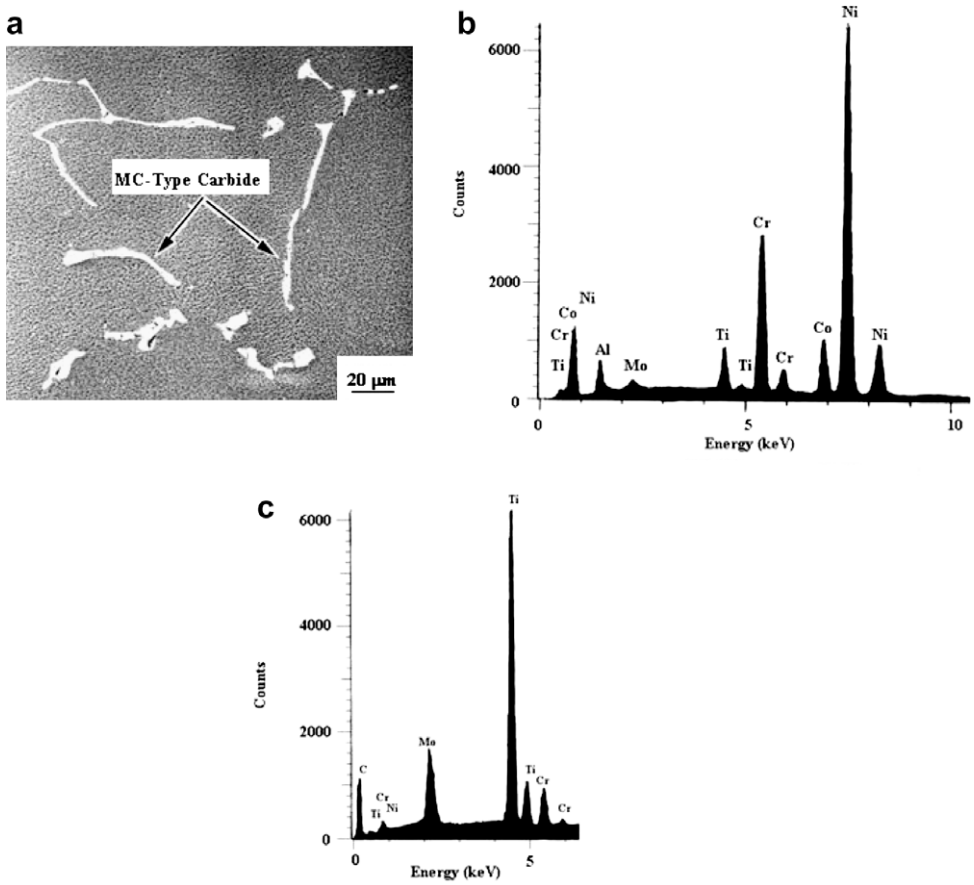

Fig. 4. Characteristic microstructural features of the blade material in the as-received condition. (a) Backscattered electron image showing a network of grain boundary carbides and the structure of γ′-phase within the matrix. (b) An energy dispersive X-ray spectrum illustrating the elemental composition of the blade alloy. (c) An energy dispersive X-ray spectrum illustrating the elemental composition of the grain boundary carbide.

Fig. 5 is a secondary electron SEM image illustrating a representative morphology of the γ′-phase near the major fractures shown in Fig. 1. Agglomeration and elongation or rafting of the γ′-phase are indicative of overheating to a level higher than the γ′-solvus temperature. It is also observed from Fig. 5 that relatively large regions of the matrix phase are free of the γ′-phase. This is further illustrated in the example of Fig. 6 derived in the scanning transmission electron microscopy (STEM) mode of an analytical electron microscope. Fig. 6a is a bright-field STEM image showing a typical microstructure of the γ′-phase at approximately halfway the distance between the two major fractures of Fig. 1. Corresponding microdiffraction pattern derived from a γ′ particle (face-centered cubic: L12 superlattice) in ⟨0 0 1⟩ orientation is shown in the inset. It is observed that the cuboidal particles of γ′-phase providing strength at higher temperatures are finer than those near the fracture surface (Fig. 5). Also, the fine spherical particles of γ′-phase providing low-temperature tensile strength are clearly distinguished. Fig. 6b is a bright-field STEM image showing typical rafting of γ′-phase near the major fractures of Fig. 1.

It is evident from the above observations that the blade was subjected to large variations in temperatures as indicated by the differences in microstructure, which could be a major factor in thermal–mechanical fatigue. Both rafting of the γ′-phase and the absence of its fine spherical particles near the major fractures are indications of overheating. Overheating was also indicated by the microstructural features of the vane material as shown below.

Fig. 7 summarizes typical microstructural features of the vane material in the as-received condition. As shown in the backscattered electron image of Fig. 7a, the grain boundaries were delineated by a continuous network of precipitates assuming a cellular-type morphology (bright contrast). Some discrete particles are also observed within the matrix phase attached to particles exhibiting darker contrast as indicated by the arrow. An example illustrating the elemental composition of the alloy is shown in the energy dispersive X-ray spectrum of Fig. 7b. Quantification of the spectral data showed that the composition is consistent with that of alloy MAR M 918 as specified.

Although the morphology of the grain boundary precipitates observed in Fig. 7a resembles the script-type morphology exhibited by MC-type carbides, detailed analysis showed that although some Ta-rich MC carbide was present, most of the precipitates consisted of Laves phase and $M_{23}C_6$ carbide to a lesser extent. An energy dispersive X-ray spectrum representative of the major portion of the grain boundary precipitates is shown in Fig. 7c. As can be seen, the major elemental con-

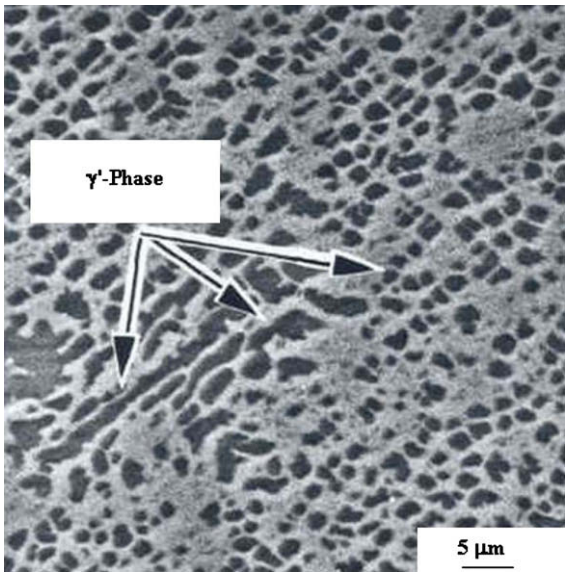

Fig. 5. Backscattered electron image illustrating coarsening and rafting of the γ′-phase in the blade material near the major fractures shown in Fig. 1 (as-received condition).

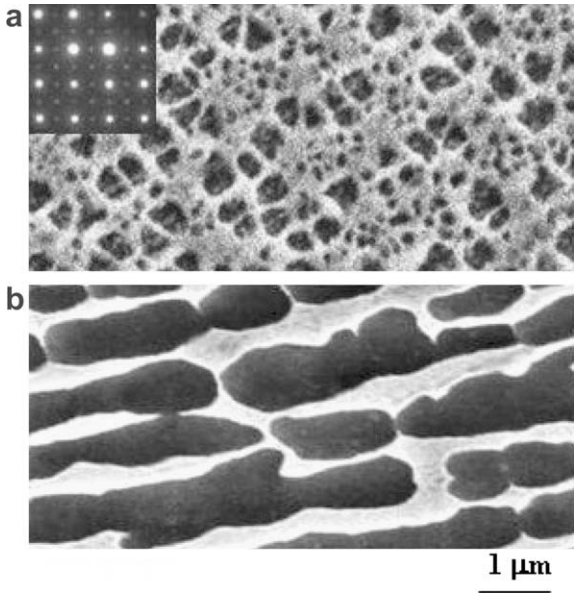

Fig. 6. An example illustrating variations in the structure of γ′-phase within the airfoil of the blade material. (a) Bright-field STEM image at a distance about halfway from the major fractures of Fig. 1 showing the presence of the cuboidal γ′ and spherical γ′ particles; the inset is a microdiffraction pattern derived from a γ′ particle in $\langle 0\,0\,1\rangle_{fcc}$ orientation. (b) Bright field STEM image showing a considerable rafting of the γ′-phase and absence of the spherical γ′ particles typical of regions near the major fracture surfaces.

stituents of the precipitates are Co, Cr, and Ta and there was no evidence for the presence of C. This was further confirmed by scanning transmission electron microscopy analysis as shown later in this section.

It is well known that Laves phase isomorphous with $MgZn_2$ (hexagonal close-packed structure: hcp) and of the type $TaCr_2$ and $TaCo_2$ are thermodynamically stable in the Co–Cr–Ta alloy system [9]. Therefore, it is possible that a solid–solution of the two phases could form resulting in a composition of the type $Ta(Co, Cr)_2$ explaining the observation of Fig. 7c. The elemental composition of the particles exhibiting dark contrast in (marked by the arrow in Fig. 7a) is shown in the spectrum of Fig. 7d consistent with the composition of a Cr-rich carbide expected to be of the type $M_{23}C_6$.

Fig. 8 is an example illustrating the results of STEM analysis of the grain boundary precipitates observed in Fig. 7a. As shown in the bright-field image of the Fig. 8a, the precipitate contained a high density of planar defects (twins and stacking

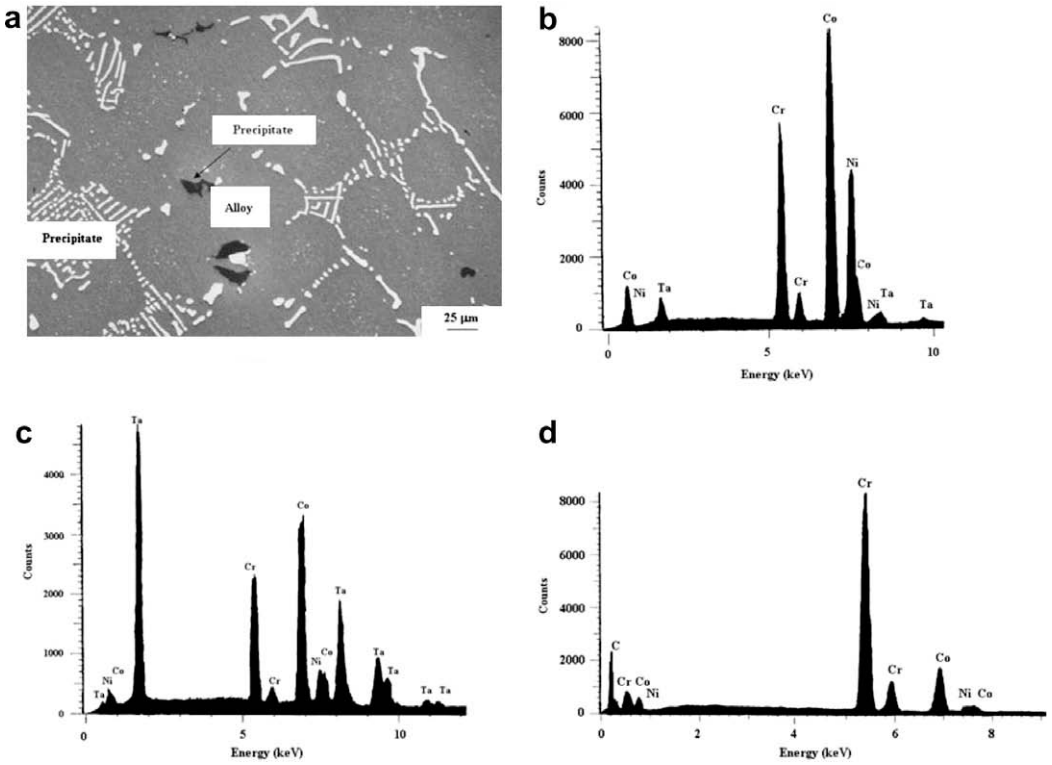

Fig. 7. Characteristic microstructural features of the vane material in the as-received condition. (a) Backscattered electron image illustrating a network of cellular precipitates at grain boundaries and scattered discrete particles within the matrix phase. (b) An energy dispersive X-ray spectrum illustrating the elemental composition of the vane material. (c) An energy dispersive X-ray spectrum illustrating the elemental composition of the grain boundary precipitates. (d) An energy dispersive X-ray spectrum illustrating the elemental composition of the matrix precipitate indicated by the arrow in (a).

faults) characteristic of topologically close-packed phases. The inset of Fig. 8a shows a corresponding electron diffraction pattern in $[0001]_{hcp}$. An energy dispersive X-ray spectrum derived from the precipitate in the STEM mode using a windowless detector is shown in Fig. 8b, which is similar to that of Fig. 7c. These results provide evidence that similar to the case of the blade described earlier, the vane was also exposed to higher than normal temperatures. Although carbides of the MC-type (Ta-rich in the present case) provide a major source for strengthening Co-base alloys, they are known to decompose at elevated temperatures [10]. This could explain at least partially, the presence of the Ta-rich Laves phase and to a lesser extent the Cr-rich $M_{23}C_6$ carbide in the vane material. It is well known that Laves phase degrades the mechanical strength of both Ni- and Co-base alloys [11].

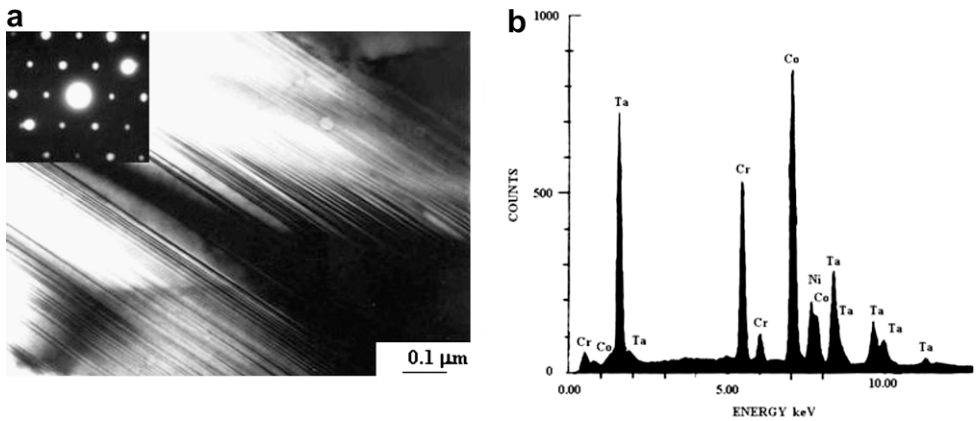

Fig. 8. An example illustrating the results of STEM analysis of Laves phase at grain boundaries of the vane material. (a) A bright-field image showing a high density of planar defects within a precipitate particle; the inset is a diffraction pattern in $[0001]_{hcp}$ orientation. (b) Corresponding energy dispersive X-ray spectrum illustrating the elemental composition of Laves phase.

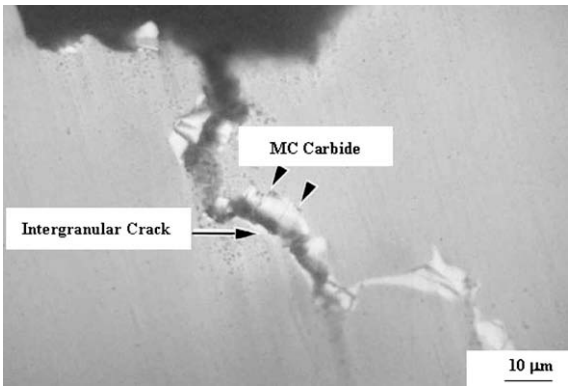

Fig. 9. Secondary electron image of a cross-section of the blade material showing an intergranular crack, and the grain boundary layer of MC carbide.

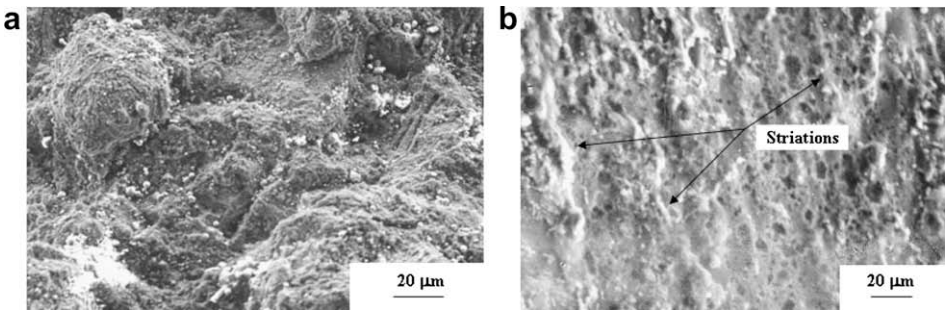

Fig. 10. Secondary electron images illustrating the fracture surface of the blade material after descaling. (a) A region showing intergranular failure. (b) A region exhibiting striations typical of fatigue failure.

3.3. Fracture mode

As pointed out earlier, extensive oxidation of the surfaces exposed by fracture of the blade and vane precluded detailed fractography. However, some morphological features could be resolved after descaling. Also, a clue about the major factors contributing to the observed fracture was obtained by examining cross-sections as shown below.

Examination of cross-sections of the fractured blade revealed the presence of secondary intergranular cracks as shown in the example of Fig. 9. This could be related to the embrittling effect of the network of grain boundary carbides degrading the creep strength. Fig. 10 summarizes some morphological features of the fracture surface revealed after descaling. In some regions of the surface, fracture appeared to occur by an intergranular mode as shown in Fig. 10a consistent with the result of

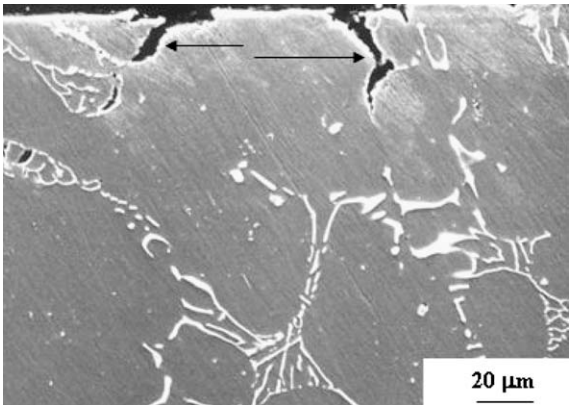

Fig. 11. Secondary electron image showing intergranular cracking along a cross-section of the vane material, as indicated by the arrows, and the network of grain boundary precipitates.

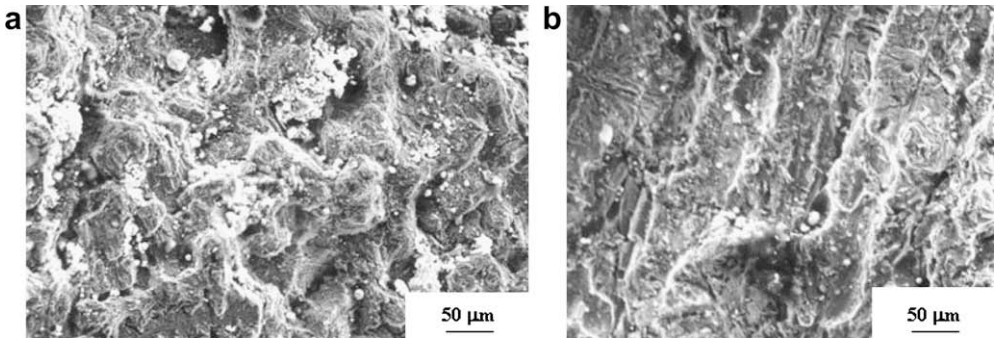

Fig. 12. Secondary electron images illustrating the fracture surface of the vane material after descaling. (a) A region exhibiting intergranular failure. (b) A region exhibiting striations typical of fatigue failure.

Fig. 9. However, other regions of the surface exhibited striations typifying fatigue failure as shown in Fig. 10b. Similar results were obtained in the case of the vane as summarized in Figs. 11 and 12. Secondary intergranular cracks were observed along cross-sections as shown in Fig. 11. After descaling, the fracture surface exhibited some features indicating that fracture occurred by a mixed mode consisting of intergranular failure and fatigue as shown in Fig. 12. It is possible that misfiring leading to large variations in temperature as indicated by the microstructural changes described earlier could have played an important role in thermal–mechanical fatigue.

Based upon the above results, it is evident that both the blade and vane were fractured by the same mechanism, which could be related to overheating degrading the thermal stability characteristics of the respective alloys and in turn their mechanical strength. Most evidence pointed out that both the blade and vane were initially damaged by creep deformation leading to a significant reduction in fatigue life.

4. Conclusion

Overheating during service was found to be responsible for fracture of the blades and vanes as determined from the observed microstructural changes, which degraded the mechanical strength of the respective alloys. Most evidence indicated that both components were fractured by a mixed mode involving creep damage and fatigue. However, creep promoted by overheating could have been the major factor in the failure because of its adverse effect on fatigue life.

Acknowledgement

It is a pleasure to acknowledge the continued support of King Fahd University of Petroleum and Minerals.

References

[1] Bernstein, H. Materials Issues for Users of Gas Turbines. In: 35th Turbomachinery Symposium, ASME IGTI Lecture, Turbomachinery Laboratory Technical Paper No. T3504ASME, Turbomachinery Laboratory, Texas A&M University, College Station, Texas, 2006.
[2] Lam M. Damage analysis of aircraft gas turbine engines. In: Dickson JI, Abramovici E, Marchand NS, editors. Failure analysis: techniques and applications. Ohio: ASM International, Materials Park; 1992. p. 137–40.
[3] Schilke PW, Foster AD, Pepe JH, Beltran AM. Advanced materials propel progress in land-based gas turbines. Adv Mater Process 1991;141(2):22.
[4] JianfuHou, Wicks Bryon J, Antoniou Ross A. An investigation of fatigue failures of turbine blades in a gas turbine engine by mechanical analysis. Eng Fail Anal 2002;9:201.
[5] Han, Je-Chin, Dutta S, Ekkad SV. Gas turbine heat transfer and cooling technology. New York, New York: Taylor and Francis; 2000. 13.
[6] O.Morocutti, editor. A guide to the control of high temperature corrosion and protection of gas turbine materials. Luxembourg: Commission of the European Communities; 1986. p. 3.
[7] Ross EW, Sims CT. In: Sims CT, Stoloff NS, Hagel WC, editors. Superalloys II. New York: John Wiley and Sons; 1987. p. 111.
[8] Wallwork G, Croll JA. Review of the strengthening mechanisms in iron and nickel based Fe–Ni–Cr alloys used at high temperatures. In: Newkirk JB, editor. Reviews of high temperature materials. London: Freund Publishing House; 1976. p. 79.
[9] Wallwork G, Croll JA. Review of the strengthening mechanisms in iron and nickel based Fe-Ni-Cr alloys used at high temperatures. In: Newkirk JB, editor. Reviews of high temperature materials. London: Freund Publishing House; 1976. p. 108.
[10] Beltron AM. In: Sims CT, Stoloff NS, Hagel WC, editors. Superalloys II. New York, New York: John Wiley and Sons; 1987. p. 144–8.
[11] Sims CT. In: Sims CT, Stoloff NS, Hagel WC, editors. Superalloys II. New York, New York: John Wiley and Sons; 1987. p. 221–6.